Eruption constraints on tube-fed planetary lava flows

Susan E. H. Sakimoto
Geodynamics Branch, Code 921, NASA/Goddard Space Flight Center, Greenbelt, MD 20771

Joy Crisp
Jet Propulsion Laboratory, California Institute of Technology, 4800 Oak Grove Drive, Pasadena, CA 91109

Stephen M. Baloga
Proxemy Research Inc., 20528 Farcroft Lane, Laytonsville, MD 20882.

Revised version for the Journal of Geophysical Research—Planets

December, 1996

Abstract.

We examine the role of pressure and gravity as driving forces in planetary lava tubes for Newtonian and power law rheologies. The tubes are assumed to have been filled with lava that was emplaced in constant diameter circular tubes in the laminar flow regime and had constant density, heat capacity, thermal conductivity, and viscosity. Our model provides relationships between tube dimensions, driving forces, and effusion rates and rheology parameters. In general, the pressure term in the driving force dominates for very small slopes, but the gravity term eclipses the pressure term as the slope increases. Applying the model to Alba Patera tube flows suggests effusion rates somewhere between 2 and 10^5 m^3/s, and viscosities between 10^2 and 10^6 Pa s, with tighter constraints (2 to 4 orders of magnitude) for specific tube sizes and travel times. These effusion rate results are lower and the viscosity ranges higher than those found in previous studies. This allows eruptions that are closer in style to terrestrial basaltic eruptions, although the flows are still considerably larger in scale than the Hawaiian tube flows. We find that very low lava viscosities are not essential for Alba Patera lava tubes, and that tube formation may be a better indicator of the steadiness of the eruption and the presence of low slopes than it is of low viscosities (e.g. 10^2 Pa s) . In addition, this analysis suggests that the tube systems on the steep flanks of Olympus Mons are fundamentally different from those at Alba Patera. The Olympus Mons flows could not have roofed over, been continuously full, or maintained a continuous lava tube transport system in the assumed full, steady, and fully developed conditions.

Introduction

Tube-fed lava flows are a significant part of the volcanic geologic record on the Earth, Mars, and possibly Venus and Io. On the flanks of Tharsis shield volcanoes on Mars, Viking images clearly show lava flows with evidence for tubes (Carr et al., 1977). Low ridge-shaped flows with central collapse pits indicative of tube-fed flow can be traced for distances of 20-30 km, which is comparable to lengths of Hawaiian lava tube flows. Alba Patera images reveal much larger lava tube flows on its NW and SE flanks (Cattermole, 1987; Cattermole, 1990; Schneeberger and Pieri, 1991). These long tube flows have been studied carefully by several authors (Carr et al., 1977; Cattermole, 1987; Cattermole, 1990; Schneeberger and Pieri, 1991). In many cases, chains of collapse pits along these flows can be easily identified typically for tens or hundreds of kilometers. Other, more moderate-scale lava flows that appear to have been at least partially tube-fed can be found at Syrtis Major (Schaber, 1982; Hodges and Moore, 1994) and Elysium Mons (Greeley, 1973; Hodges and Moore, 1994). While the cooling dynamics are very different from those on the Earth and Mars, it has been suggested that tube-fed flows extending tens to hundreds of kilometers exist on Venus as well (for example, see Gregg and Greeley, 1993). Tube flows on volcanically active Io are also a possibility (Crown et al., 1992). Some lobate flows emanating radially from central calderas (e.g., Ra and Maasuw Pateras) suggest tube-fed flow, although the resolution of Voyager images limits this to conjecture.

In this work, we develop a basic fluid dynamic model for planetary tube-fed lava flows. The model is applied to tube flows at Alba Patera and Olympus Mons, Mars. The Viking Orbiters acquired images of tube-fed flows in both regions with resolutions of 70 to 100 meters per pixel. The lava tube flows in Alba Patera flow over slopes estimated to be less than half a degree, while the Olympus Mons tube flows considered here are on slopes of 5° to 34° and can be traced for 20 to 30 km (Carr, 1981). In both cases, the lengths of the tubes are inferred from the extent of the chains of central collapse pits where the tube roof has collapsed. These collapse depressions are typically 1 to 5 pixels (70 to 500 m) across. Even with allowance for a collapse pit width that is greater than the underlying tube, the data presently available suggest tube radii of at least many tens of meters.

On the Earth, the existence of tube-fed flow is usually indicative of a long eruption duration and a stable discharge rate. However, many eruptions do not produce extensive lava tubes or tube systems for a variety of reasons. For example, eruption duration has to be sufficiently long for the constructional process to be completed and extended over a significant reach. Also, dramatic changes in the eruption rate do not provide sufficient stability in the flow field for a tube to form and persist. It should also be noted that there have been no documented cases of tube flow in compositions more silicic than andesites.

Pressure plays an important role in the flow and emplacement of basaltic lava tubes. In tube flow, there are frequent signs that the lava is locally under high pressure. Tumuli in tube-fed pahoehoe flow fields, rootless vents, and dome fountaining at tube breakouts all indicate a pressurized delivery system. Pahoehoe sheet flows in Hawaii are often inflated after their initial emplacement to many times their initial thickness by lava delivered from the tube system into the still molten interior of the flow (Hon et al., 1994).

Pressure-driven flows have also been suggested since many of the longest known lava tubes are on less than 1° slopes. These include the 160 km Undara flow and nearby flows in Queensland, Australia (Atkinson, Griffin and Stephenson, 1975; Stephenson and Griffin, 1976), the 75 km Carrizozo flow field in New Mexico (Keszthelyi and Pieri, 1993), and the 200 to 300 km long tube flows of Alba Patera, Mars (e.g. Cattermole, 1990). Pressure features, such as tumuli and dome-shaped flow sections, have been documented in some of these low-slope flows (Carr et al., 1977; Keszthelyi and Pieri, 1993). These observations prompt questions of the possible role of pressure as a dominating force influencing flow length and flow morphology.

We will explore potential ranges and limitations on the distribution of pressurization within lava tubes, such as those observed at Alba Patera and Olympus Mons. The model we develop features a relationship between the pressure field and flow parameters such as the effusion rate, viscosity, lava tube diameter, and slope. We examine three regimes of tube-flow: pressure-driven, gravity-driven, and combined pressure- and gravity-driven flow and consider both Newtonian and power law rheologies. When no slope is present, the flow is what we call "pressure-driven" from the tube entrance, with a pressure drop vs. distance along the tube that is a function of the flow rate, tube radius, and viscosity.

Since the roof and surrounding wall rock is of limited tensile strength, the maximum length of such a flat tube segment can be constrained assuming typical values of strength for a jointed rock mass. This is done for a range of tube sizes, flow rates, and tube diameters estimated from images of the collapse pits. Alternatively, for any given tube length and radius the eruption rate and flow viscosity may be constrained.

The addition of an underlying slope to the problem allows two additional types of flow models. The simplest is what we call "gravity-driven" tube flow, where the fluid pressure is hydrostatic at all points along the path of the flow and gravity supplies the only driving force. This situation can be caused by flow over steep topographic slopes that makes the pressure gradient in the Navier-Stokes equation negligible compared to the external gravitational force. In "combined flow", both the pressure gradient and gravitational forces are significant and must be considered simultaneously.

This consideration of driving forces in lava tube flow analysis allows us to explore the relative importance of pressure and gravity and to provide some new constraints on the planetary eruption conditions that produced particular lava tube flows, and we demonstrate this for a variety of tube flows and slopes on Olympus Mons and Alba Patera volcanoes. The results also are presented in a general form for use on other planetary basaltic provinces.

Theory and Approach

Assumptions

For this study, we would like to predict the velocity distribution, maximum and average velocities, and volume rate of flow for both Newtonian and power law rheologies. We use the coordinate system shown in Figure 1, where r is the radial coordinate, z is the axial coordinate, and θ is the slope. We assume that the flow is isothermal and incompressible with a constant viscosity, and that it is steady, laminar, fully developed, and flowing in a full, straight, constant radius, circular tube with smooth walls. We consider the effects of varying viscosity, tube size and length, slope, and driving pressure on effusion rate.

Any of these assumptions could be challenged for some subset of flow conditions. In addition to noting that the assumptions simplify the analysis, there are some observations to substantiate them. First, lava tube formation is more likely in steady flow conditions (constant eruption rate), since some stability is necessary to form a tube floor and maintain it (Peterson et al., 1994). Second, a constant density is an important simplifying assumption, although there is some evidence for significant changes in vesicularity along the path of the flow (Swanson and Fabbi, 1973; Cashman et al., 1994). Third, the flow is assumed to be laminar, with a circular tube and constant cross section. While analytic solutions are available for other constant cross section shapes such as ellipses and rectangles (e.g. Shah and London, 1978; White, 1991), the possible differences in flow rates due to the assumption of a circular cross section are small compared to other uncertainties in this work. For example, using the flow rate expressions of White (1991), we find that even ellipses and rectangles with axial length/width ratios of 10 still have flow rates within a magnitude of the circular tube flow rate for the same driving pressure, hydraulic diameter (D_h = 4(area)/(perimeter)), viscosity, and tube length.

The assumption of constant cross section along the flow length is made since we lack any information besides collapse pit size. The assumption of a full tube may be questioned, since lava tubes are often seen running partially full at a small fraction of their potential flow rate. However, all lava tubes must have run full at some point in order for the roof to form, so long as the base of the tube has not been eroded. Consequently, the constraints from this study are for the maximum eruption rates (or minimum eruption durations), which may have been transient.

The assumption of fully developed flow means that the velocity profile in the tube does not change with distance along the path of the flow, while the assumption of steady flow means that the flow does not vary with time. For a straight circular tube and laminar flow, the distance necessary to reach steady, fully developed flow is given by the expression

$$\frac{L_e}{D} = \frac{0.60}{0.035\,\mathrm{Re}+1} + 0.056\,\mathrm{Re} \qquad (1)$$

(Shah and London, 1978; equation 195), where L_e is the hydrodynamic entrance length, D is the lava tube diameter, and Re is the dimensionless Reynolds number ($Re = \rho VD/\mu$). Since laminar flow ceases around Re = 2000–3000 for smooth tubes, L_e is limited to at most 100 diameters (White, 1991).

However, for a 100 m diameter lava tube, this can be as much as 10 km, which is a significant fraction of planetary tube lengths. The potential errors incurred by assuming fully developed flow within the entrance length are estimated in the discussion section.

Velocity distribution

For the assumptions in this model, we desire a velocity distribution. A standard momentum balance analysis for steady, incompressible, laminar, fully developed flow in a straight tube of constant circular cross section yields the momentum flux distribution (shear as a function of strain rate) (Bird et al., 1960)

$$\tau_{rz} = \mathcal{P}\frac{r}{2}. \tag{2}$$

Here $\mathcal{P}$ is the total driving force per unit volume

$$\mathcal{P} = \frac{\Delta P}{L} + \rho g \sin(\theta), \tag{3}$$

in terms of the pressure gradient and the gravitational body force. For a Newtonian fluid, the shear–strain rate relationship is linear, and we have

$$\tau_{rz} = -\mu\frac{dv_z}{dr} \tag{4}$$

where μ is the viscosity An v_Z is the flow velocity in the z direction. We can substitute equation (4) into equation (2) to obtain a differential equation for velocity

$$\frac{dv_z}{dr} = -\frac{\mathcal{P}}{2\mu}r \tag{5}$$

which is integrated to produce

$$v_z = -\frac{\mathcal{P}}{4\mu}r^2 + C. \tag{6}$$

The integration constant C is determined by the noting that the velocity must be zero at the tube wall ($v_z = 0$ at $r = a$). The Newtonian velocity distribution is then

$$v_z = \frac{\mathcal{P}}{4\mu}a^2\left[1-\left(\frac{r}{a}\right)^2\right]. \tag{7}$$

The same procedure may be used to obtain the velocity distribution for power law flow. The corresponding power law shear–strain rate relationship is

$$\tau_{rz} = K\left(-\frac{dv_z}{dr}\right)^n \tag{8}$$

(Bird et al., 1960; Skelland, 1967) where K is the fluid consistency index (also called the power law coefficient) with units of kg $s^{n-2}m^{-1}$, and n is the flow behavior index (sometimes called the power law exponent) which is dimensionless. If equation (8) is substituted into equation (2), integrated, and rearranged, we obtain the power law velocity distribution.

$$v_z = \frac{na}{n+1}\left(\frac{a\mathcal{P}}{2K}\right)^{\frac{1}{n}}\left[1-\left(\frac{r}{a}\right)^{\frac{n+1}{n}}\right] \tag{9}$$

(Skelland, 1967). Equations (7) and (9) may be written in terms of pressure-driven flow (no slope), gravity-driven flow (no pressure) or combined flow by keeping the relevant terms in (3) and then inserting it into equation (7) or (9).

Flow rate, mean velocity, and flow type

Given the velocity distributions of equations (7) and (9), we can find several geologically useful quantities. The mean velocity V is obtained by integrating the velocity distribution over the cross section and dividing by the cross sectional area (Bird, 1960), and is

$$V = \frac{\mathcal{P}}{8\mu}a^2 \tag{10}$$

for Newtonian flow and

$$V = \frac{na}{3n+1}\left(\frac{a\mathcal{P}}{2K}\right)^{\frac{1}{n}} \tag{11}$$

for power law flow (Skelland, 1967). The volume rate of flow is simply the average velocity multiplied by the cross section area, and is

$$Q = \frac{\pi a^4 \mathcal{P}}{8\mu} \tag{12}$$

for Newtonian flow and

$$Q = \frac{n\pi a^3}{3n+1}\left(\frac{a\mathcal{P}}{2K}\right)^{\frac{1}{n}} \tag{13}$$

for power law flow (Skelland, 1967).

Substitution of equation (3) into equation (12) yields the flow rate expression

$$Q = \frac{\pi a^4}{8\mu}\left[\frac{\Delta P}{L} + \rho g \sin(\theta)\right]. \tag{14}$$

When there is no slope, a confined viscous fluid requires a pressure-gradient to maintain the flow. Thus, internal pressure drops systematically along the path of the flow. In this work, we consider only a constant pressure gradient. If all other factors are held constant, except for the values of the pressure gradient and the inclination of the tube, the constant pressure gradient has its maximum value when the slope is zero.

When the underlying slope is not zero, the gravitational body force contributes to the flow rate according to the steepness of the slope. When the flow is maintained more by the pressure gradient then the gravitational force on the fluid, we will refer to it as "pressure-driven". When the gravitational force on the fluid contributes more to the flow rate than the pressure gradient, we will refer to it as "gravity-driven".

The end member of gravity-driven flow features a pressure gradient that is negligible compared to the gravitational term. (Clearly some finite slope is necessary.) This means that the pressure in the tube is the constant hydrostatic value. If we imagine a tube on an inclined plane, small flow rates will not fill the tube and the flow will be laminar provided that the Re number is sufficiently small. The pressure will be hydrostatic with no gradient over the tube length, no matter how long the tube is. Gravity-driven flow cannot be used as a constraint on the length of the tube. As we increase the flow rate, making sure the RE stays below the critical value, the tube will fill, but will still be completely gravity -driven like any open channel laminar flow. Once the tube is just filled, we have a purely gravity driven flow in a full tube with a constant flow rate and pressure at all points along the flow.

To obtain a higher flow rate, additional pressure must be applied at the entrance of the tube. This pressure drops systematically along the length of the tube as in the pressure-driven regime. When both

the pressure gradient and gravitational forces are comparable in their contribution to the flow rate, we refer to the situation as "combined flow". In this mixed regime, we have

$$L = \frac{\Delta P}{\frac{8\mu Q}{\pi a^4} - \rho g \sin(\theta)} \tag{15}$$

which becomes infinite for the case of purely gravity-driven flow.

Table 1 shows equations (12) and (13) with equation (3) substituted for $\mathcal{P}$ in pressure-driven flow ($\mathcal{P} = \Delta P/L$), gravity-driven flow ($\mathcal{P} = \rho g \sin(\theta)$), and combined flow ($\mathcal{P} = \Delta P/L + \rho g \sin(\theta)$). They are indicated in the Table as equations N1-N8 for Newtonian flow, and P1-P8 for power law flow. Equations N3 and P3 for the pressure drop are simply rearrangements of N1 and P1, respectively. Next, we will consider pressure-driven and gravity-driven Newtonian flow, and then illustrate the differences between the power law and Newtonian rheology solutions.

Pressure-driven flow

For pressure-driven flow on a flat surface, we can combine equation N3 and the tensile failure strength of terrestrial jointed basalt, ΔP_{crit}, to predict when the pressure within the tube, ΔP, ought to exceed the strength of the tube at the tube roof. When $\Delta P \geq \Delta P_{crit}$, a breakout and effective truncation of the tube system is assumed. Since a range of 0.1 to 2.5 MPa has been experimentally found for ΔP_{crit} in jointed basalt (Schultz, 1995), failure is expected somewhere in this range. This failure data is for 2 to 4 meters of basalt, and therefore this model is for near-surface tubes. Note that, with a standard lava density of 2600 kg/m^3, mars gravity of 3.81 m/s^2, and a 100 m tube, the hydrostatic pressure at the bottom of the tube is 10^6 Pa.

For the flow analysis, tube length and radius are either measured from a specific tube, or taken as averages or representative values for a set of tubes in a region. Effusion rates from 1 to 10^6 m^3/s and viscosities of 10^2 to 10^5 Pa s are considered. These parameters are used with equation N3 in Table 1 to plot required driving pressure vs. effusion rate for each viscosity (Figure 2). The plot area above the 2.5 MPa jointed strength upper limit is considered to be a regime in which tube flow is not allowed. The area between the 0.1 and 2.5 MPa strength values is considered to be a possible tube flow regime, and the area below the 0.1 MPa limit is considered to be a likely tube flow regime. We further bound the

flow regime by considering only laminar flow, since turbulent flow has not been observed in terrestrial lava flows, and we do not know if, as an essentially different flow regime, it would produce the same final flow morphologies. Turbulent flow may have been present, but the effusion rate and flow equations are quite different for turbulent flow, so this model is not valid in that regime. The laminar ($Re \leq 2000$), transitional ($2000 \leq Re \leq 3000$), and turbulent flow ($Re \geq 3000$) regimes are added to the pressure vs. effusion rate plots. An additional bound for the effusion rate is provided by assuming a minimum effusion rate of 1 m^3/s, which was chosen as a minimum because it represents a low flow rate for small Hawaiian tube flows (e.g. Peterson et al., 1994).

For specific tube sizes, the lower bound on effusion rate can be constrained further by assuming minimum average travel times for the lava through the tube. The average travel time is the time it takes lava at the average flow velocity to travel the length of the tube, and is directly related to the effusion rate ($t_{ave} = L/V = L\pi a^2/Q$) for any tube length and radius. Reasonable upper limits for travel times can be chosen on the basis of terrestrial experience with basaltic eruptions.

If desired, a viscosity vs. effusion rate plot for each tube length and diameter can also be constructed. They are omitted here since the information is also contained in the driving pressure vs. effusion rate plots, but they may be useful for individual flow analysis. We then substitute the flow rate vs. velocity ($V=Q/\pi a^2$) expression into the Reynolds number, and solve for viscosity to obtain

$$\mu = \frac{2\rho Q}{\mathrm{Re}\,\pi a}. \tag{16}$$

Equation (16) is substituted into equation N3 to get the pressure at the flow transition in terms of the constraints and the flow rate

$$\Delta P = \frac{16}{\mathrm{Re}} \frac{\rho L Q^2}{\pi^2 a^5} \tag{17}$$

so that when $Re = 2000$,

$$\Delta P_{\mathrm{Re}=2000} = \frac{16}{2000} \frac{\rho L Q^2}{\pi^2 a^5}, \tag{18}$$

which is repeated to obtain the $Re = 3000$ flow regime boundary. This requires the assumption of a flow density, but yields an allowed flow regime where the flow is laminar and the tube does not break for any

given combination of tube length and diameter. This allowed flow regime can be shown as a region in a plot of viscosity vs. effusion rate for each tube length and diameter. This is done by plotting equation (16) with $\Delta P = 2.5$ MPa for the upper viscosity bound, and $\Delta P = 0.1$ MPa for the lower viscosity bound for flow within the tensile failure pressure range of the tube. For flow below the tensile failure pressure range, $\Delta P = 0.1$ MPa is the upper viscosity bound, and equation (18) is the lower viscosity bound.

Gravity-driven flow

For gravity-driven flow, the ΔP term in equations N7 and N8 in Table 1 is zero, and we obtain equations N4 and N5. The model set up is similar to that used for pressure-driven flow; tube length and radius are measured and effusion rates from 1 to 10^6 m^3/s are considered along with viscosities of 10^2 to 10^5 Pa s. Then equation N4 in Table 1 is rearranged to yield required slope vs. effusion rate for each viscosity

$$\theta = \arcsin\left(\frac{8\mu Q}{\pi a^4 \rho g}\right). \tag{19}$$

The boundaries of the laminar and turbulent regimes are found by substituting equation (16) into equation (19) to yield

$$\theta = \arcsin\left(\frac{16}{\mathrm{Re}}\frac{Q^2}{\pi^2 a^5}\right), \tag{20}$$

and plotting the result for $Re = 2000$ and $Re = 3000$. A tube-fed flow that is driven purely by the gravitational term only provides the relationship

$$\mu = \frac{\pi a^4 \rho g \sin(\theta)}{8Q} \tag{21}$$

because flow is independent of a pressure gradient in this limiting case. Our assumption of laminar flow, however, provides and important upper bound on the flow rate

$$Q \le \frac{\pi a \mu}{2\rho}\mathrm{Re}. \tag{22}$$

Figure 3 illustrates the relationship in equation 21, and the constraint of equation 22.

At the opposite extreme, we will consider flow conditions (e.g., radii, density, and viscosities) that produce a minimum effusion rate of 1 m^3/s. The minimum travel times discussed in the previous section indicate that any lower effusion rates produce unreasonable long emplacement times for flows of the planetary dimensions considered here.

Combined flow

Combined pressure and gravity-driven flow is probably more common than either of the end members. We can consider the relative roles of pressure and gravity driving forces in combined flow by considering a lava tube of a given radius, length, flow rate, and lava viscosity, and using equation N7 of Table 1 to compare the relative magnitudes of the pressure and gravity terms for increasing slopes. If we assume a constant flow rate, tube diameter, and flow viscosity, then rearranging equation N7 yields

$$\Delta P = \frac{8\mu QL}{\pi a^4} - \rho g L \sin(\theta), \tag{23}$$

which is the pressure required at the tube entrance for the assumed flow rate for a range of slopes and tube lengths. This is plotted against the contribution to the flow rate from gravity ($\rho gLsin(\theta)$) to assess the relative importance of the two terms in various tube flows. For a tube of finite length on an inclined plane, a pressure gradient must be applied to increase the flow rate above that of the purely gravity-driven case. Equation 23 determines the pressure difference between the two ends of the tube, above the force per unit area due to the weight of the fluid column, required to produce a finite flow rate. Figure 4 illustrates the case where the additional pressure difference is very small compared to the weight of the fluid, and is plotted in terms of the slope alone.

The pressure and gravity contributions are plotted vs. slope for increasing slopes until the gravity term is sufficient to account for the entire assumed flow rate. The pressure contribution dominates for very small slopes, but the gravity contribution eclipses the pressure contribution as the slope increases. Only the pressure contribution varies with viscosity, tube diameter, flow rate, or along the tube length, so increasing viscosity, flow rate or tube length, or reducing the tube diameter increases both the pressure contribution magnitude as well as the ratio of the pressure contribution to the viscosity contribution.

Power law flow

Other rheology models besides Newtonian have often been suggested for basaltic lavas, particularly power law and Bingham rheologies, which allow models to reproduce some of the known shear-dependent behavior of basaltic melts (e.g. Shaw et al., 1968; Pinkerton and Sparks, 1978; Hardee and Dunn, 1981; Pinkerton and Norton, 1995; Sakimoto, 1995). Non-Newtonian rheologies need a minimum of two rheology parameters such as yield strength and plastic viscosity for Bingham flow, or flow consistency (K) and power law exponent (n) for power law flow. The magnitudes of both parameters generally increase with decreasing temperature.

The same approach can be used to investigate the difference between non-Newtonian and Newtonian rheologies on flow rate for selected power law rheology parameters. If specific non-Newtonian rheology parameters are chosen, this approach yields the non-Newtonian flow rates that can be compared to the Newtonian flow rates. For example, Hardee and Dunn (1981) proposed two power law rheologies for Shaw's 1135°C basalt data (Shaw et al., 1968). Figure 5 shows the velocity profiles for a 50 m diameter tube on a 0.1° slope. Each power law velocity profile and associated mean velocity results in a flow rate (equations P7 and P8 in Table 1). The Newtonian velocity profile and associated viscosity for the same tube and flow rate is plotted with each power law velocity profile for comparison. For these rheology parameters, the effect of the power law rheology is small compared to other uncertainties in the analysis.

Alba Patera Tube Flow

Alba Patera is a very large low relief central vent volcanic structure on the northern portion of the Tharsis bulge of Mars. The summit is about 7 km above the Mars datum plains, and the diameter is estimated to be 1600 km (Carr, 1981). The average slopes for Alba Patera are estimated to be less than half a degree (Carr, 1981) with steeper slopes near the summit and shallower slopes on the outer flanks (Cattermole, 1990). Alba Patera is characterized by many examples of well-preserved flow features, including well defined lobate surface lava flows as well as a multitude of lava tube ridges and channels up to hundreds of kilometers long (Carr et al., 1977; Cattermole, 1987, 1990; Mouginis-Mark et al.,

1988; Schneeberger and Pieri, 1991, Hodges and Moore, 1994). The vast sizes of the lava flows as well as the extremely shallow slopes have led to suggestions that Alba Patera lavas were rather fluid basalts erupted at effusion rates of 103 to 106 m3/s (Cattermole, 1987, 1990).

The long tube flows at Alba Patera have a ridged cross section (Cattermole, 1990, Schneeberger and Pieri, 1991), generally 6-10 km wide (Cattermole, 1987) where the flow margins can be resolved. They may extend up to several hundred kilometers in length, and many have a central chain of collapse pits or an axial channel if they have been completely unroofed (Cattermole, 1987, 1990). Figure 6 shows several lava tube flows on the NW flanks of Alba Patera. Several chains of collapse pits are visible along tube axes, and the flow margins are difficult or impossible to pick out. Figure 7 shows an example of a lava tube flow with visible margins and collapse pits. The flow can be traced through several images, and is at least 220 km long with widths ranging from 7 to 18 km. Some of the Alba Patera lava tubes show signs of lava under pressure within the tube, such as the one in Figure 8, where several dome-like features are visible (Carr et al., 1977), which are reminiscent of terrestrial basaltic tumuli.

Since there are many long tube flows on Alba Patera, we have selected representative tube lengths of 200 and 50 km. For tube diameters, we have examined many of the high resolution images for the tube-fed flows at Alba Patera. Pixel resolution is 70 to 100 m for most of the images available, with 10 m per pixel resolution available for a few areas. Where collapse pits can clearly be identified, we find definite visual evidence of them as regions perpendicular to the flow direction that are one to five pixels wide in the 70 to 100 m per pixel images, and five to fifteen pixels wide for the 10 m per pixel images. Consequently, we consider tens of meters to a hundred meters to be a representative dimension for these structures. For the purpose of our analysis, tube diameters are assumed to be 50m and 100m, approximately the same size as the collapse pits.

The pressure-driven flow results for Alba Patera are shown in Figure 2. Each plot corresponds to one of the assumed combinations of diameters and lengths, and shows pressure vs. effusion rate. We have indicated in the plots the turbulent flow region as well as where we expect the roof of a tube to reach its tensile failure strength, and these serve as the upper boundaries on the effusion rate. The transition between laminar and turbulent flow is quite narrow even for smooth tubes, but it is indicated on the plots also. For lower effusion rate boundaries, we assume a minimum pressure head of 0.01 MPa

(this is quite small—the equivalent approximately to a one meter column of lava). We also stipulate maximum tube travel times of either 100 days or 1000 days, which can be refined as additional cooling estimations are available. For example, for Figure 2a (where L=200km and D=100m), 0.04 MPa at the tube source and a flow viscosity of 10^3 Pa s will drive an effusion rate of 300 m^3/s over a flat surface with an average travel time of less than 60 days.

For the same flow rate, a larger tube diameter allows flows with higher viscosities to be transported downstream. For this mode of flow, a wide range of viscosities and flow rates are possible even if the flow is restricted to the laminar regime, although the flow rates are lower than those previously estimated by Cattermole (1987, 1990). For the 50 m diameter tubes (Figure 2b, 2d), flow rates are restricted to less than approximately 10^4 m^3/s for stronger jointed rock, and 10^3 m^3/s for the weaker jointed rock. For the 100 m diameter tubes (Figure 2a, 2c), flow rates are restricted to less than approximately 10^5 m^3/s for stronger jointed rock, and 10^4 m^3/s for the weaker jointed rock.

If we use the upper limit of 1000 days for average travel time, a tube in Figure 2a (L=200 km, D=100 m) is limited to effusion rates greater than approximately 10 m^3/s, tubes in Figure 2b (L=200 km, D=50 m) and 2c (L=50 km, D=100 m) are limited to effusion rates greater than approximately 5 m^3/s, and the tube in Figure 2d is limited to effusion rates greater than approximately 1 m^3/s. A tighter constraint of 100 days average travel time yields lower effusion rate limits of approximately 200 m^3/s for Figure 2a, 50 m^3/s for Figures 2b and 2c, and 10 m^3/s for Figure 2d. If we further consider the possibility that the tubes could be much smaller than their collapse pit diameters, the flow rates could be even smaller. For example, if Figure 2a is recalculated for a 25 m diameter tube (around 1/4 the collapse pit width), the flow rates may be limited to less than approximately 1000 m^3/s for stronger jointed rock, and less than 300 m^3/s for the weaker jointed rock. Viscosities for both tube diameters are shown as high as 10^5 or 10^6 Pa s in Figure 2. We consider these high viscosities to be plausible upper bounds given the simplicity of the assumptions and terrestrial experience. Basaltic lavas on Earth with such viscosities are highly crystalline, and their viscosities are sensitive to small temperature changes, but changes in viscosity along the path of the flow are beyond the scope of this analysis.

The same tube lengths and diameters are considered in gravity-driven flow for Alba Patera tubes. We assume density to be 2600 kg/m^3, and gravitational acceleration to be 3.7m/s^2. Slopes at Alba

Patera are poorly constrained, estimated to average less than 0.5°(Carr et al., 1977). Estimates of the flank slopes have yielded smaller values of 0.01°–0.02° (Cattermole, 1990), and even shallower slopes may be present. However, even shallow slope estimates yield interesting results (Figure 3). A slope of 0.001° will drive a tube flow for viscosities ranging from 10^2 to 10^6 Pa s, and effusion rates of 1 to 10^5 m^3/s (depending on tube diameter and length).

For combined (gravity-driven dominating) flow and tube diameters of 50 and 100 m and lengths of 50 and 200 km, slopes above 0.1° result in predicted failure of the tube roof (Figure 4). However, higher slopes could be sustained for shorter tube lengths or larger tubes. As for pressure-driven flow, we can add lower constraints on the effusion rate with an average travel time limit, and also add a lower slope limit. Here we assume that the regional slope must be at least 0.01°(which is only 35 m of vertical rise over 200 km of flow) in order to overcome local topographic variations. Subsequent work on local topographic roughness vs. regional slopes may help clarify where this break between local and regional slope influences is most likely to be. A 1000 day upper limit on average travel time yields lower effusion rate limits of 20, 5, 5, and 1 m^3/s, for the tubes in Figures 4a, 4b, 4c, and 4d, respectively. The 100 day time limit results in lower effusion rate limits of 200, 50, 50, and 10 m^3/s for Figures 4a, 4b, 4c, and 4d, respectively. The minimum slope assumption raises these lower limits to the 2-20 m^3/s range and, combined with the laminar flow assumption, eliminates most flows with viscosities of 10^2 Pa s from consideration as pure gravity-driven flows.

For the combined flow analysis for Alba Patera, we initially consider the relative roles of pressure and gravity driving forces in combined flow by considering a lava tube of a given radius, length, flow rate, and lava viscosity, and use equation (23) to compare the relative magnitudes of the pressure and gravity contributions for an assumed flow rate for increasing slopes. Figure 9 shows the pressure-driven and gravity-driven terms vs. slope in combined tube flow for a 100 m diameter tube with a flow viscosity of 10^3 Pa s for tube lengths of 50 and 200 km, and flow rates of 10^3 and 10^4 m^3/s. In both plots, the lines are terminated where the slope is sufficient for the gravity term to account for all of the flow rate, which can be found from equation N4 in Table 1. As expected, the pressure contribution dominates for very small slopes, but the gravity contribution eclipses the pressure contribution as the slope increases. For the same tube sizes and flow viscosities as Figure 9, but with

lower flow rates (e.g. 1 to 100 m^3/s), the gravity contribution dominates on all but the smallest slopes (e.g. 0.001 °), and the flow is effectively a gravity-driven flow. While Figure 9 illustrates the simple trade-off between slope and pressure applied to the lava at the tube head, it is a comparison of maximum values for the pressure and gravity terms, which will vary over the tube length.

To consider variations in total internal pressure along a tube in combined flow, we consider a 50m diameter tube with a flow viscosity of 10^3 Pa s, and the pressure-driven, gravity-driven, and combined flow regimes (see Figure 10). For pressure-driven flow, a flow rate of 10^3 m^3/s on Mars requires 1.3 MPa at the tube entrance in order drive the flow through a 200 km tube length. For comparison, this is the pressure at the base of a 135 meter column of lava or rock at a density of 2600 kg/m^3. For gravity-driven flow, a slope of 0.04° (135 m elevation change over 200 km) and no applied pressure at the tube entrance for the same tube would result in the same flow rate of 10^3 m^3/s. For combined flow, half the slope (0.02°) and half the entrance pressure (0.65 MPa) can combine to produce the same flow rate of 10^3 m^3/s. For all three flow cases the resulting flow rate is the same, but the pressure measured along the top of the tube interior would be different. For the pressure-driven flow, the pressure would start at 1.3 MPa and drop to zero at the tube end (relative to ambient pressure); for gravity driven flow the pressure would start at zero and rise to 1.3 MPa (from the weight of the lava upstream); and for the combined flow above, the total pressure would remain at 0.65 MPa over the entire tube length. It is apparent from Figure 10 that flow with the driving forces evenly split between gravity and pressure produces the pressure field over the flow length with the lowest maximum values, and thus is the least likely to break out of the tube for a given flow rate. For these "half-and-half" combined flows, the pressures and slopes required for a particular flow rate, tube length and tube diameter are simply half those of the purely pressure-driven or gravity-driven flows. Consequently, evaluating a tube flow as a either a solely pressure-driven or solely gravity-driven flow in the narrow range of slopes where both processes are important may underestimate the maximum flow rate. However, if either the pressure or gravity forces produce a tube-top pressure within the tensile failure range, consideration of combined flow is not going to substantially lengthen the maximum possible flow length.

Table 2 shows the summary of all of the Alba Patera tube flow results. We have combined the analyses so that the effusion rates encompass the ranges predicted for pressure-driven, gravity-driven, and combined flows. The lower viscosity lavas (10^2 Pa s) produce turbulent flow for all gravity-driven cases considered, but only a few of the pressure-driven cases. Table 2 does not include the turbulent flow cases, only the laminar pressure-driven ones. The effusion rates and viscosities span a large range for all of the Alba Patera tubes considered (2 to 10^5 m^3/s, and 10^2 to 10^6 Pa s, respectively). Selecting a particular tube size and maximum travel time narrows the ranges by one or two orders of magnitude. Generally, though, the viscosity ranges in Table 2 center on values of approximately 10^3 Pa s, and effusion rate ranges center on values of around a few hundred to a few thousand m^3/s, with variations for individual tube geometries. This is consistent with the basaltic compositions suggested for Alba Patera (e.g. Carr et al., 1977; Cattermole, 1987), although the effusion rates are generally lower than the 10^5 to 10^6 m^3/s suggested by Cattermole (1990). These lower effusion rate estimates and higher viscosity estimates allow eruptions that are closer in style to terrestrial basaltic eruptions than those suggested by Cattermole, although the flows are still considerably larger in scale than the familiar Hawaii tube flows. Some of the lower viscosities suggested by Cattermole (e.g. 10^2 Pa s, 1987) are not in the probable viscosity ranges for many of the tubes considered here, since they would result in turbulent flow. Low lava viscosities are not essential at Alba Patera, and tube formation may be a better indicator of the steadiness of the eruption and the presence of low slopes then it is of low viscosities.

Olympus Mons Tube Flow

Olympus Mons is the highest volcano on Mars, with a height of 23 km from the surrounding plains, a diameter over 500 km, mean slopes of 4°, and a steep basal scarp up to 6 km high (e.g. Carr, 1981; Cattermole, 1992). The volcano flanks have a radial fabric narrow flows interpreted to be of leveed, channel, and lava tube flows, with some of these draped over the steep basal scarp (Carr, 1981).

Figure 11 shows several lava tube flows draped over the NE Olympus Mons scarp. At least one of the flows (the central of the three) continues for a few kilometers onto the surrounding plains. These flows are only 11 to 25 kilometers long and are approximately 5 km wide. They are much smaller than

the Alba Patera tube flows, and were emplaced on much steeper slopes. We calculated the topographic slopes from the Mars Global Digital Topography for a straight transect along each of the three lava tubes indicated in Figure 11. Figure 12a shows the topography and the approximate locations of the lava tubes along the transect. The slope ranges in Figure 12a are calculated from the transect data for 3 km intervals. Figure 12b shows the transect locations and the Olympus Mons scarp, and the endpoint coordinates are listed in the caption for Figure 12a. In general, the slopes for the upper lava tube sections are 5–9°, while the slopes along lava tube scarp sections are 25–34°.

For flows on Olympus Mons which have been suggested to be tube-fed, the estimates of the tensile strength of jointed basalt are low enough that, for current estimates of Olympus slopes, the hydrostatic pressure alone should have been sufficient to break the roof of the tube before the observed tube length was reached. For these slopes, the gravity term will be much larger than the pressure term, resulting in gravity-driven flow. However, if we consider equation (22) for the case where the second term on the right is much greater than the 1st term on the right (gravity-dominated combined flow), we can predict a maximum full tube length of

$$L_{max} = \frac{\Delta P_{crit}}{\rho g \sin(\theta)} \tag{24}$$

where L_{max} is the maximum length of the full tube or tube segment . Equation (24) indicates that the lava tubes could have been full for less than a few kilometers at a time for the 5-9° slopes just above and below the Olympus Mons scarps, and for less than a kilometer at a time for the steeper 25-34° scarp slopes. There are no obvious breakout flows from the proposed tubes visible at this image resolution, and the center "collapse pits" are closer in appearance to a continuous sinuous depression than the chains of isolated pits seen at Alba Patera and on many terrestrial tube flows. These Olympus Mons flows were probably not the classic type of tube-fed flow, and may instead have been tube-like with a roofing-over levee accretion and arch building process like that of the Mauna Ulu flows described in Peterson et al. (1994), but with the roof formation having stopped before it was completed. A possible terrestrial analog is shown in R. Greeley's photo of a Mauna Ulu flow printed in Hodges and Moore (1994, page 43). This analysis does not rule out the possibility of tube flow in short full segments of the tube during construction, with later flow along the entire tube, as long as it was only partially full.

We find that, for Olympus Mons, this model predicts that the steeper slopes would have caused the internal tube pressure to quickly exceed the roof strength if the tubes were full. We conclude that either the tubes were normally partially full, and were never full over their entire length at once, or that the proposed tube flows were probably not the classic type of tube-fed flow with a continuous roof. Also possible, although less likely, is that the material was stronger than the assumed terrestrial jointed basalt. In either case, this model is inappropriate for effusion rate estimations.

Discussion

This approach to lava tube flow analysis allows estimation of effusion rate ranges for pressure-driven, gravity-driven, and combined flows, if some reasonable assumptions are made for failure strength, flow regime, travel time, and minimum slope or pressures. The method can be applied to Newtonian flows, and the results will constrain viscosity ranges with effusion rates (as is demonstrated here), or it can be applied to power law flows, where the method will constrain power law coefficients and exponents along with effusion rates.

Entrance length effects

Previously, we noted that for some conditions, planetary flows might have a substantial portion of their length within the hydrodynamic entrance length. For such undeveloped flows, applying the fully developed assumption of this model will lead to errors in flow rate predictions. Here we consider how large those errors are likely to be for planetary flows. If we use the entry length of equation (1), assume Newtonian flow, and then substitute flow rate for velocity ($V=Q/\pi a^2$, a = tube radius) in the Reynolds number, we obtain

$$\frac{L_e}{D} = \frac{0.60}{0.035\left(\rho QD/\mu\pi a^2\right)+1} + 0.056\left(\rho QD/\mu\pi a^2\right) \qquad (25)$$

which is plotted in Figure 13 as entrance length vs. flow rate for a variety of viscosities and tube diameters. Figure 13a is for a tube diameter of 10 m and viscosities ranging from 10^2 to 10^5 Pa s, and Figure 13b is for a tube diameter of 100 m.

From Figure 13, we can see that smaller tubes ($D \leq 10$m) have entrance lengths of 1 km or less, and fully developed flow is thus a good assumption for long tube flows (>10 km). For 100 m diameter tubes, the entrance length is also fairly small (a few hundred meters or less) for flow rates less than around 100 m^3/s, and fully developed flow is a good assumption here also. However, for the 100 m diameter tubes and flow rates greater than 100 m^3/s, the laminar flow regime allows entrance lengths of up to ten kilometers. For these larger tubes, fully developed flow is a poorer assumption for the low viscosity flows unless the tube is quite long (e.g., 50-100 km).

An estimate of how poor the fully developed assumption is can be made by comparing entrance length pressure drop and flux rates to those predicted under the fully developed flow assumption. The pressure drop over the hydrodynamically developing length,

$$\frac{\Delta P}{\frac{1}{2}\rho V^2} = C_{f,app}\frac{4z}{D} \tag{26}$$

can be calculated with a formula developed by Shah (1978; also see White, 1991, equation 4-177 and table 4-7; Bejan, 1995, equation 3-117) for the apparent friction $C_{f,app}$

$$C_{f,app}\,\mathrm{Re} = \frac{3.44}{\sqrt{\zeta}} + \frac{C_f\,\mathrm{Re} + 1.25/4\zeta - 3.44/\sqrt{\zeta}}{1 + 0.000212/\zeta^2} \tag{27}$$

where C_f is the fully developed flow friction factor, and $C_f Re = 16$ for a circular pipe. ζ is the dimensionless axial distance $\left(\zeta = (z/D)/\mathrm{Re}\right)$. Equation (27) is thought to be accurate to within ± 2% (Shah, 1978). If we substitute $C_f Re = 16$ and the ζ expression into equation (27), and then substitute equation (27) into equation (26), we obtain an expression for pressure drop within the entrance length

$$\frac{\Delta P}{\frac{1}{2}\rho V^2} = 13.74\sqrt{\zeta} + \frac{1.25 + 64\zeta - 13.74\sqrt{\zeta}}{1 + 0.000212/\zeta^2} \tag{28}$$

(Bejan, 1995). The pressure drop in the entrance section can also be written as

$$\Delta P_{entr} = \Delta P_{dev}\frac{C_{f,app}\,\mathrm{Re}}{16} \tag{29}$$

where $C_{f,app}$ is calculated from equation (27), ΔP_{entr} is the pressure drop evaluated in the entrance section, and ΔP_{dev} is the pressure drop for the same tube, evaluated assuming fully developed flow. Similarly, the volume flux in the entrance section is

$$Q_{entr} = Q_{dev} \frac{16}{C_{f,app}\,Re}. \qquad (30)$$

Figure 14 is a plot of $\Delta P_{entr}/\Delta P_{dev}$ and Q_{entr}/Q_{dev} for Re of 2000, 1000, and 100. It is interesting to note that volume flux is a function of tube length in developing flow. For both the pressure drop and the volume flux, the worst errors we can incur by assuming developed flow are less than 10% for 50 km long tubes even for flows with Re = 2000 and L_e = 11 km. For a 10 km tube and a Reynolds number of 2000, the volume flux over the entrance section is 30% lower than we would predict for fully developed flow, and the pressure drop is 30% higher. Thus, even for flows where the entire flow length is slightly shorter than the predicted entrance length, the errors are less than 30%, which is within the uncertainty we will encounter for other variables such as tube diameter and slope.

Conclusions

This simple analysis of tube flow shows the relationships between tube dimensions, driving forces, and effusion rates and rheology parameters. For representative values of L, r, θ, and t, the analysis of tube flows at Alba Patera tube flows suggests an effusion rate range between 2 and 10^5 m^3/s, and viscosities between 10^2 and 10^6 Pa s. These effusion rate estimates are lower than those found in previous studies, while the viscosity ranges are slightly higher for most tubes, and include a larger range. We conclude that low lava viscosities are not essential at Alba Patera, and tube formation may be a better indicator of the steadiness of the eruption and the presence of low slopes than it is of low viscosities. In contrast, this analysis suggests that the tube systems on the steep flanks of Olympus Mons are fundamentally different than those at Alba Patera. The Olympus Mons flows could not have roofed over or maintained a continuous lava tube transport system in the assumed full, steady, and fully developed conditions. As is apparent from the wide ranges of effusion rate and viscosity, our current knowledge of the lava tube sizes, slopes, and lava travel times only provide limited constraints. The Mars Surveyor laser altimeter (MOLA, Zuber et al., 1992), and imaging camera (MOC, Malin et al., 1992) will be able to provide detailed regional topography, topographic flow profiles and lava flow imaging. This will substantially improve the accuracy of the slope and tube size estimates at Alba Patera

and Olympus Mons, as well as providing additional morphologic evidence at Olympus Mons to help resolve the issues of flow steadiness and open channel vs. tube flow. Until then, the simple physics of this model can explain the long lava tube flows of Alba Patera as similar to conventional terrestrial steady tube flow, but fails at Olympus Mons, where either the model assumptions are inappropriate or the flows were emplaced by fundamentally different physical processes.

Acknowledgments

This research was performed while S. Sakimoto held a National Research Council Research Associateship at NASA's Goddard Space Flight Center. Contributions by S. Baloga were performed at Proxemy Research under a grant from the National Aeronautics and Space Administration. The work by J. Crisp was performed at the Jet Propulsion Laboratory, California Institute of Technology, under a contract with the National Aeronautics and Space Administration.

References

Atkinson, A., T.J. Griffin, and P.J. Stephenson, A major lava tube system from Undara Volcano, North Queensland, *Bulletin of Volcanology*, *39*, 266-293, 1975.

Baloga, S., P.D. Spudis, and J.E. Guest, The dynamics of rapidly emplaced terrestrial lava flows and implications for planetary volcanism, *Journal of Geophysical Research*, *100* (B12), 24509-24519, 1995.

Bejan, A., *Convection Heat Transfer, 2nd Ed.*, 623 pp., John Wiley and Sons, New York, 1995.

Bird, R.B., W.E. Stewart, and E.N. Lightfoot, *Transport Phenomena*, 780 pp., John Wiley and Sons, New York, 1960.

Carr, M.H., *The Surface of Mars*, 232 pp., Yale University Press, New Haven, 1981.

Carr, M.H., R. Greeley, K.R. Blasius, J.E. Guest, and J.B. Murray, Some Martian volcanic features as viewed from the Viking Orbiters, *Journal of Geophysical Research*, *82*, 3985-4015, 1977.

Cashman, K.V., M.T. Mangan, and S. Newman, Surface degassing and modifications to vesicle size distributions in active basalt flows, *Journal of Volcanology and Geothermal Research*, *61*, 45-68, 1994.

Cattermole, P., Sequence, rheological properties, and effusion rates of volcanic flows at Alba Patera, Mars, *Journal of Geophysical Research*, *92*, E553-E560, 1987.

Cattermole, P., Volcanic development at Alba Patera, Mars, *Icarus*, *83*, 453-493, 1990.

Cattermole, P., *Mars, The Story of the Red Planet*, 224 pp., Chapman and Hall, London, 1992.

Crown, D.A., R. Greeley, R.A. Craddock, and G.G. Schaber, Geologic Map of Io, Map I-2209, 1:15,000,000, United States Geological Survey, 1992.

Dragoni, M., A. Piombo, and A. Tallarico, A model for the formation of lava tubes by roofing over a channel, *Journal of Geophysical Research, 100* (B5), 8435-8447, 1995.

Greeley, R., Observations of actively forming lava tubes and associated structures, Hawaii, *Modern Geology*, *2*, 207-223, 1971.

Greeley, R., Additional observations of actively forming lava tubes and associated structures, Hawaii, *Modern Geology*, *3*, 157-160, 1972.

Greeley, R., Mariner 9 photographs of small volcanic structures on Mars, *Geology*, 175-180, 1973.

Gregg, T.K.P., and R. Greeley, Formation of Venus canali: Considerations of lava types and their thermal behaviors, *Journal of Geophysical Research, 98* (E6), 10873-10882, 1993.

Hardee, H.C., and J.C. Dunn, Convective heat transfer in magmas near the liquidus, *Journal of Volcanology and Geothermal Research*, *10*, 195-207, 1981.

Hodges, C.A., and H.J. Moore, Atlas of volcanic landforms on Mars, *U.S. Geological Survey Professional Paper*, *1534*, 194 pp., 1994.

Hon, K., J. Kauahikaua, R. Denlinger, and K. Mackay, Emplacement and inflation of pahoehoe sheet flows: Observations and measurements of active lava flows on Kilauea Volcano, Hawaii, *Geological Society of America Bulletin*, *106* (March), 351-370, 1994.

Keszthelyi, L.P., and D.C. Pieri, Emplacement of the 75-km-long Carrizozo lava flow field, south-central New Mexico, *Journal of Volcanology and Geothermal Research, 59*, 59-75, 1993.

Malin, M.C., G.E. Danielson, A.P. Ingersoll, H. Masursky, J. Veverka, M.A. Ravine, and T.A. Soulanille, Mars Observer Camera, *Journal of Geophysical Research, 97*, 7699-7718, 1992.

Mouginis-Mark, P.J., L. Wilson, and J.R. Zimbelman, Polygenic eruptions on Alba Patera, Mars, *Bulletin of Volcanology*, *50*, 361-379, 1988.

Peterson, D.W., R.T. Holcomb, R.I. Tilling, and R.L. Christiansen, Development of lava tubes in the light of observations at Mauna Ulu, Kilauea Volcano, Hawaii, *Bulletin of Volcanology*, *56*, 343-360, 1994.

Pinkerton, H., and G. Norton, Rheological properties of basaltic lavas at sub-liquidus temperatures: laboratory and field measurements on lavas from Mount Etna, *Journal of Volcanology and Geothermal Research*, *68* (Nov.), 307-324, 1995.

Pinkerton, H., and R.S.J. Sparks, Field measurements of the rheology of lava, *Nature*, *276*, 383-385, 1978.

Schaber, G., Syrtis Major: A low-relief volcanic shield, *Journal of Geophysical Research*, *87* (B12), 9852-9866, 1982.

Schneeberger, D.M., and D.C. Pieri, Geomorphology and stratigraphy of Alba Patera, Mars, *Journal of Geophysical Research*, *96* (B2), 1907-1930, 1991.

Schultz, R.A., Limits on strength and deformation properties of jointed basaltic rock masses, *Rock Mechanics and Rock Engineering*, *28* (1), 1-15, 1995.

Shah, R.K., A correlation for laminar hydrodynamic entry length solutions for circular and noncircular ducts, *Journal of Fluids Engineering*, *100*, 177-179, 1978.

Shah, R.K., and A.L. London, *Laminar Flow Forced Convection in Ducts*, 477 pp., Academic Press, New York, 1978.

Shaw, H.R., T.L. Wright, D.L. Peck, and R. Okamura, The viscosity of basaltic magma: An analysis of field measurements in Makaopuhi lava lake, Hawaii, *American Journal of Science*, *266* (April), 225-264, 1968.

Skelland, A.H.P., *Non-Newtonian Flow and Heat Transfer*, 469 pp., Wiley, New York, 1967.

Stephenson, P.J., and T.J. Griffin, Some long basaltic lava flows in North Queensland, in *Volcanism in Australasia*, edited by R.W. Johnson, pp. 41-51, Elsevier, New York, 1976.

Swanson, D.A., and P.B. Fabbi, Loss of volatiles during fountaining and flowage of basaltic lava at Kilauea Volcano, Hawaii, *Jour. Research U.S. Geol. Survey, 1* (6), 649-658, 1973.

White, F.M., *Viscous Fluid Flow*, 614 pp., McGraw-Hill, New York, 1991.

Zuber, M.T., D.E. Smith, S.C. Solomon, D.O. Muhleman, J.W. Head, J.B. Garvin, J.B. Abshire, and J.L. Bufton, The Mars Observer Laser Altimeter Investigation, *Journal of Geophysical Research, 97* (E5), 7781-7797, 1992.

Figure Captions

Figure 1. Coordinate system used for tube flow analysis. z is the axial coordinate, r is the radial coordinate, a is the tube radius, and θ is the slope of the tube.

Figure 2. Pressure-driven tube flow results (ΔP vs. effusion rate) for tubes of different lengths and diameters for Alba Patera. The dark gray region is laminar flow at pressures below the tensile failure of jointed basalt, the lighter gray region is laminar flow at pressures within the tensile failure range of jointed basalt. The thick black line corresponds to the laminar to turbulent transition zone, and the width of the line is slightly thicker than the width of the zone. The upper x axis is the average time for lava to travel the length of the tube. For a) through c), the tube length L and the tube diameter D are indicated on the plot.

Figure 3. Slope vs. effusion rate and viscosity for combined flow where the pressure-driven contribution is much smaller than the gravity-driven contribution. The light gray area is laminar flow, the dark gray area is transitional flow and the white area is turbulent flow. A) is for a tube diameter of 50 m, and b) is for a tube diameter of 100 m.

Figure 4. Gravity-driven tube flow results for Alba Patera (slope vs. effusion rate) for tubes of different lengths and diameters for Alba Patera. The dark gray region is laminar flow at pressures below the tensile failure of jointed basalt, the lighter gray region is laminar flow at pressures within the tensile failure range of jointed basalt. The thick black line corresponds to the laminar to turbulent transition zone, and the width of the line is slightly thicker than the width of the zone. The upper x axis is the average time for lava to travel the length of the tube. For a) through c), the tube length L and the tube diameter D are indicated on the plot.

Figure 5. Velocity vs. radial distance from the tube centerline $(r/a = 0)$ to the wall $(r/a = 1)$ for a 50 m diameter tube on a 0.1° slope for two power law rheologies proposed by Hardee and Dunn (1981) using data on Hawaiian basalts (Shaw et al., 1968). Each pair of velocity profiles is for an assumed power law rheology (solid line), and the Newtonian profile (dashed line) that

would result from the same flow rate. For the top pair of profiles, the flow rate is 2370 m^3/s, and for the bottom pair, 1253 m^3/s.

Figure 6. Examples of lava tube flows on the NW flanks of Alba Patera, Mars. Several long ridged flows with central chains of collapse pits are visible and indicated by arrows. Viking Orbiter Image 007B24, with image center of approximately 47.5°N, 118°W. Resolution is 94 m/pixel, a ten kilometer scale bar is shown at the bottom of the image. Collapse pit features typically range from 1 to 7 pixels across. The Patera summit is towards the lower left of the image, and North is towards the upper right.

Figure 7. Example of a lava tube flow with easily visible margins and collapse pits. Viking Orbiter Image 252S01, with image center of approximately 47.5°N, 116°W. Resolution is 71 m/pixel, a ten kilometer scale bar is shown at the bottom of the image. This flow is easily traced through several orbiter images (Viking Orbiter Images 252S03, 252S05).

Figure 8. Lava tube flow on the NW flanks of Alba Patera with several dome-like features (Carr et al., 1977). They are reminiscent of tube-fed tumuli on Earth, and may indicate pressurized conditions within the tube system. Viking Orbiter image 007B47, with image center at approximately 46.5°N, 124°W. Resolution is 93 m/pixel.

Figure 9. Comparison of pressure-driven and gravity-driven terms in combined tube flow results for Alba Patera. All plots are for 100 m diameter tube with a flow viscosity of 10^3 Pa s, and show pressure-driven flow contribution (solid curves) and gravity-driven flow contribution (dashed lines) vs. slope angle. a)Tube length of 200 km, flow rate of 10^3 m^3/s. b) Tube length of 200 km, flow rate of 10^4 m^3/s. c) Tube length of 50 km, flow rate of 10^3 m^3/s. d) Tube length of 50 km, flow rate of 10^4 m^3/s. The plots are terminated where the slope is sufficient for the gravity term to account for all (>99%) of the flow rate. The gray areas are the tensile failure range for jointed basalt. Note the scale differences for the y-axes.

Figure 10. Internal pressure at the top of the lava tube vs. distance from the tube entrance for a 50 meter diameter tube with a flow viscosity of 10^3 Pa s and a flow rate of 10^3 m^3/s under Mars gravity. The gray box is the tensile failure strength range of jointed basalt, and in plots b, c, and d, the solid line is the total internal tube pressure at the tube top, the dashed line is the pressure-driven flow contribution, and the dotted line is the gravity-driven flow contribution. a) The solid line is the total internal tube pressure for pressure-driven flow, the dashed line is the total internal tube pressure for gravity-driven flow on a slope of 0.04°. b) Combined flow with a slope of 25% of that in a. c) Combined flow with a slope of 50% of that in a. d) Combined flow with a slope of 75% of that in a.

Figure 11. Lava flows draped over the Olympus Mons scarp. Three probable tube flows and their lengths are indicated on the image. Viking Orbiter Image 047B25 (resolution of 85 m/pixel), figure center approximately 21.5°N, 130.5°W. Location image of Olympus Mons from shaded relief image MG15N127. As at Alba Patera, Collapse pit features typically range from 1 to 7 pixels across.

Figure 12. a) Topographic profiles for straight transect along three lava tubes from figure 10. The reported slopes were averaged over 5 pixel segments along the profile. The topography and profile fit data are from the Mars Global Digital Image and Topography files MG15N127 and TG15N127. b) Tube profile locations (image location is indicated on image 047B25). Profile A–A' has endpoint locations and elevations of (131.306°W, 21.586°N, 12249 m) and (130.975°W, 22.492°N, 4874 m). Profile B–B' has endpoints of (131.221°W, 21.555°N, 12454 m) and (130.853°W, 22.336°N, 4976 m). Profile C–C' has endpoints of (130.323°W, 21.133°N, 12351 m) and (129.663°W, 21.852°N, 4054 m).

Figure 13. Entrance lengths for lava tubes as a function of flow rate for four viscosities. Entrance length is calculated from equation (25) for a tube diameter of (A) 10 m and (B) 100m and each of the four viscosities (in Pa s.) indicated on the plot. The gray area designates the turbulent flow regime.

Figure 14. Pressure drop and volume flux vs. tube length and Reynolds number in and near the tube's hydrodynamic entrance length. Results are normalized with the fully developed flow results, and plotted as $DP_{entr}/\Delta P_{dev}$ (dashed lines) and Q_{entr}/Q_{dev} (solid lines) vs. tube length for Re of 2000, 1000, and 100 with entrance lengths of 11.2, 5.6, and 0.57 km, respectively.

Table 2.: Summary of approximate effusion rate ranges for pressure-driven, gravity-driven and combined laminar lava tube flow on Mars for several viscosities, tube lengths, and tube sizes typical of Alba Patera tube flow. Slopes are assumed to be ≥ 0.01 °, and driving pressures ≥ 0.01 MPa.

Tube Length [km]	Viscosity [Pa s]	Tube diameter [m]	Effusion Rate Range for $t_{ave} \leq$ 1000 days [m^3/s]	Effusion Rate Range for $t_{ave} \leq$ 100 days [m^3/s]
200	10^2	100	1000–5000	1000–5000
	10^3		100–$3x10^4$	200–$3x10^4$
	10^4		20–3000	200–3000
200	10^2	50	80–3000	80–3000
	10^3		8–2000	40–2000
	10^4		4–200	40–200
50	10^2	100	—	—
	10^3		600–$1x10^5$	600–$1x10^5$
	10^4		30–$1x10^4$	40–$1x10^4$
50	10^2	50	200–2000	200–2000
	10^3		20–8000	20–8000
	10^4		2–700	10–700

Table 1.: Volume flow rate and mean flow velocity for pressure-driven, gravity-driven, and combined (pressure- and gravity-driven) flow, for Newtonian and power law rheologies, in laminar flow conditions for a circular tube.

	Newtonian	**Power Law**
Cylindrical Tube Flow:		
Pressure-driven		
volume flow rate	$Q = \frac{\pi a^4 \Delta P}{8 \mu L}$ (N1)	$Q = \frac{n \pi a^3}{3n+1}\left(\frac{a \Delta P}{2LK}\right)^{\frac{1}{n}}$ (P1)
mean velocity	$V = \frac{a^2 \Delta P}{8 \mu L}$ (N2)	$V = \frac{na}{3n+1}\left(\frac{a \Delta P}{2LK}\right)^{\frac{1}{n}}$ (P2)
pressure drop	$\Delta P = \frac{8 Q \mu L}{\pi a^4}$ (N3)	$\Delta P = \frac{2 Q^n K L}{\pi^n a^{3n+1}}\left(\frac{3n+1}{n}\right)^n$ (P3)
Gravity-driven		
volume flow rate	$Q = \frac{\pi a^4 \rho g \sin(\theta)}{8 \mu}$ (N4)	$Q = \frac{n \pi a^3}{3n+1}\left(\frac{a \rho g \sin(\theta)}{2K}\right)^{\frac{1}{n}}$ (P4)
mean velocity	$V = \frac{a^2 \rho g \sin(\theta)}{8 \mu}$ (N5)	$V = \frac{na}{3n+1}\left(\frac{a \rho g \sin(\theta)}{2K}\right)^{\frac{1}{n}}$ (P5)
pressure drop	$\Delta P = 0$ (N6)	$\Delta P = 0$ (P6)
Combined		
volume flow rate	$Q = \frac{\pi a^4}{8 \mu}\left(\frac{\Delta P}{L} + \rho g \sin(\theta)\right)$ (N7)	$Q = \frac{n \pi a^3}{3n+1}\left[\frac{a}{2K}\left(\frac{\Delta P}{L} + \rho g \sin(\theta)\right)\right]^{\frac{1}{n}}$ (P7)
mean velocity	$V = \frac{a^2}{8 \mu}\left(\frac{\Delta P}{L} + \rho g \sin(\theta)\right)$ (N8)	$V = \frac{na}{3n+1}\left[\frac{a}{2K}\left(\frac{\Delta P}{L} + \rho g \sin(\theta)\right)\right]^{\frac{1}{n}}$ (P8)

Figure 4.

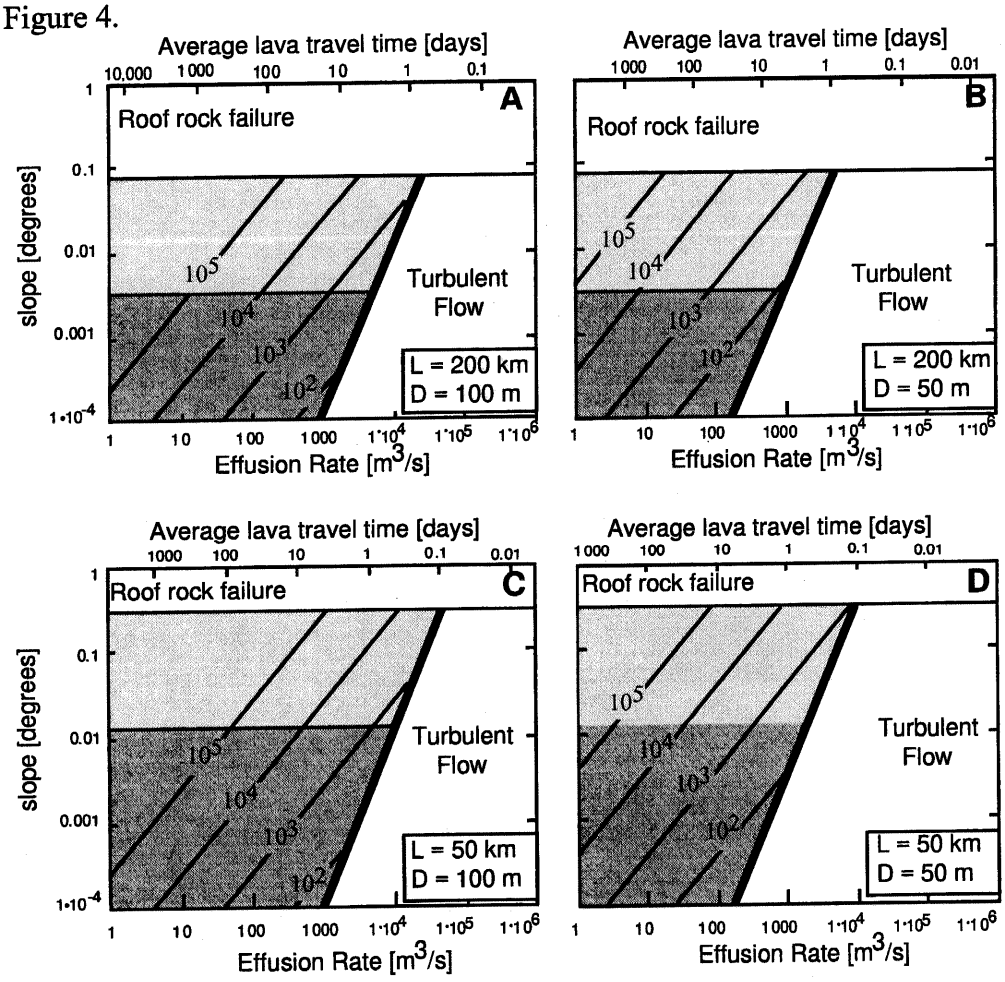

Figure 5.

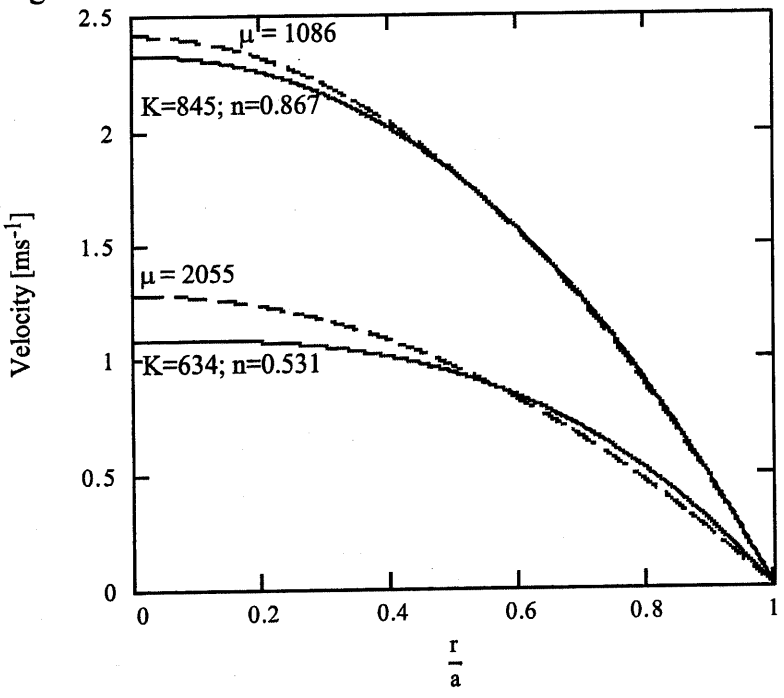

Figure 1.

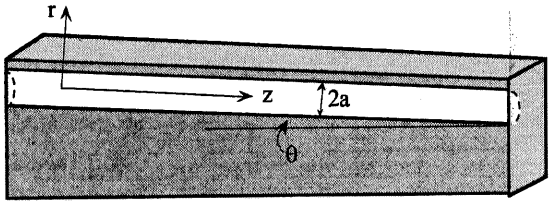

Figure 2.

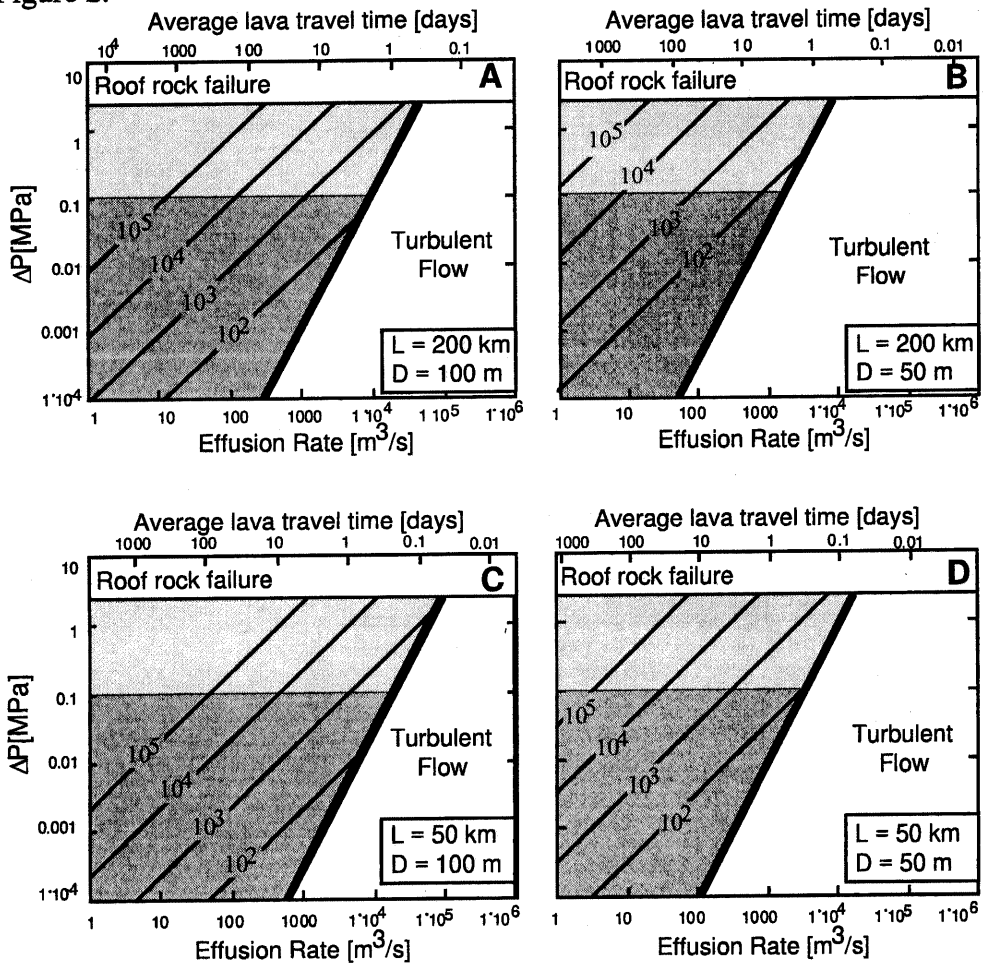

Figure 3.

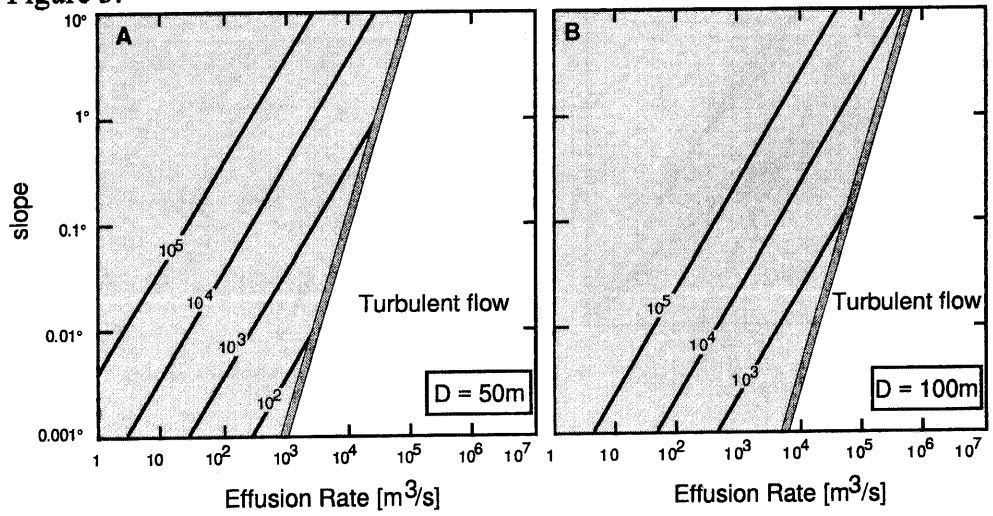

Figure 8.

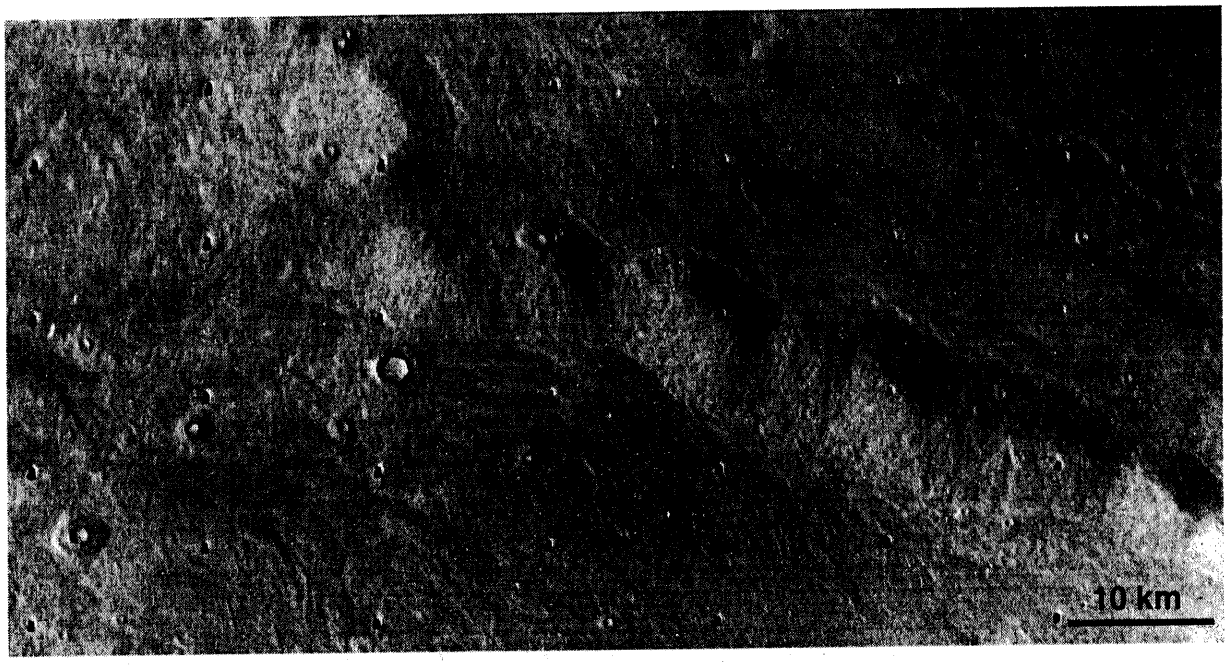

Figure 6.

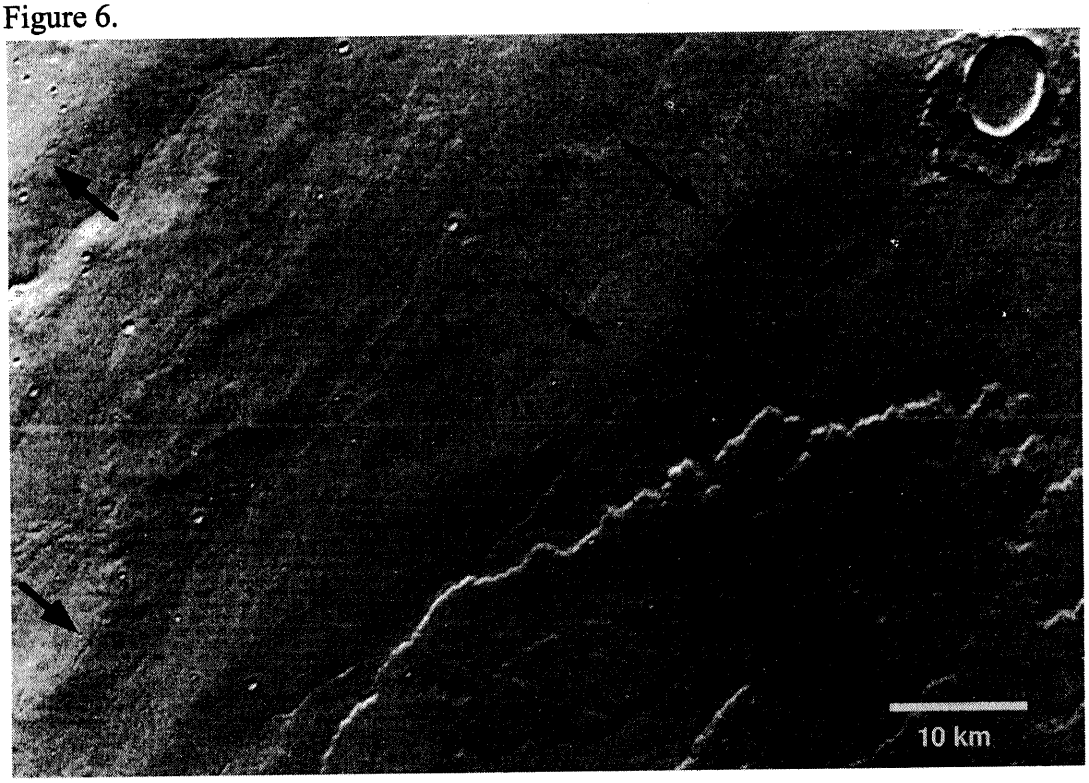

Figure 7.

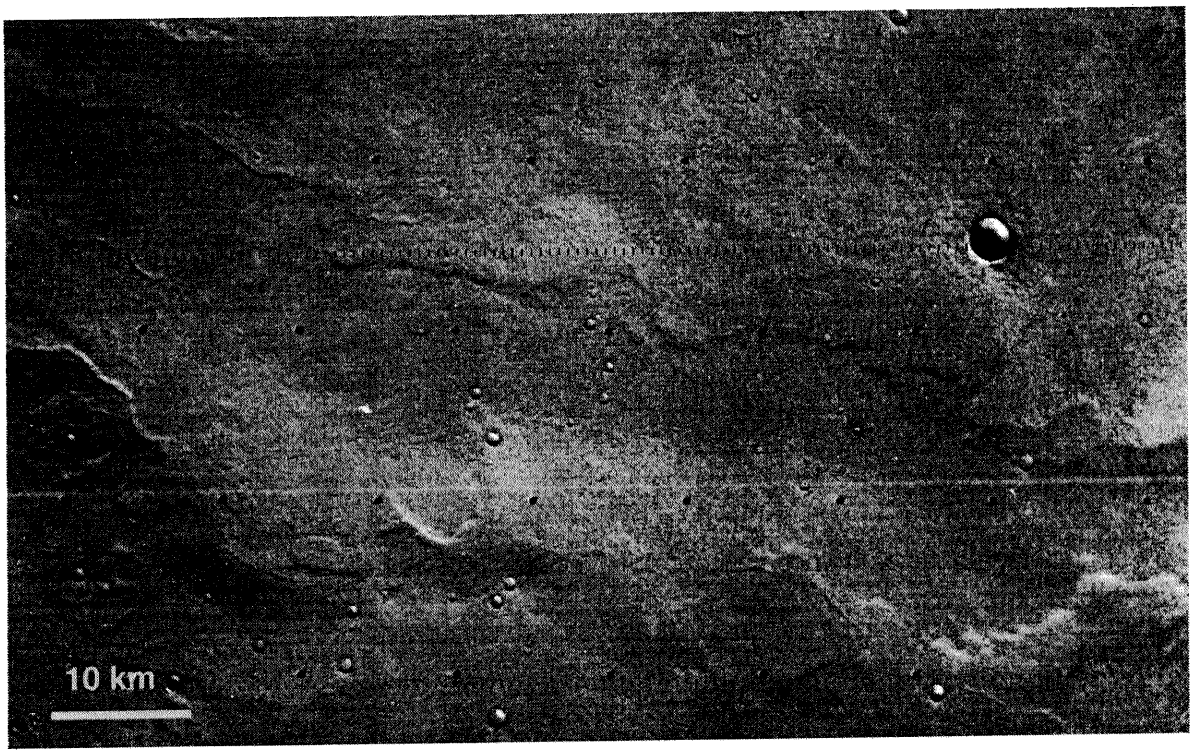

Figure 10.

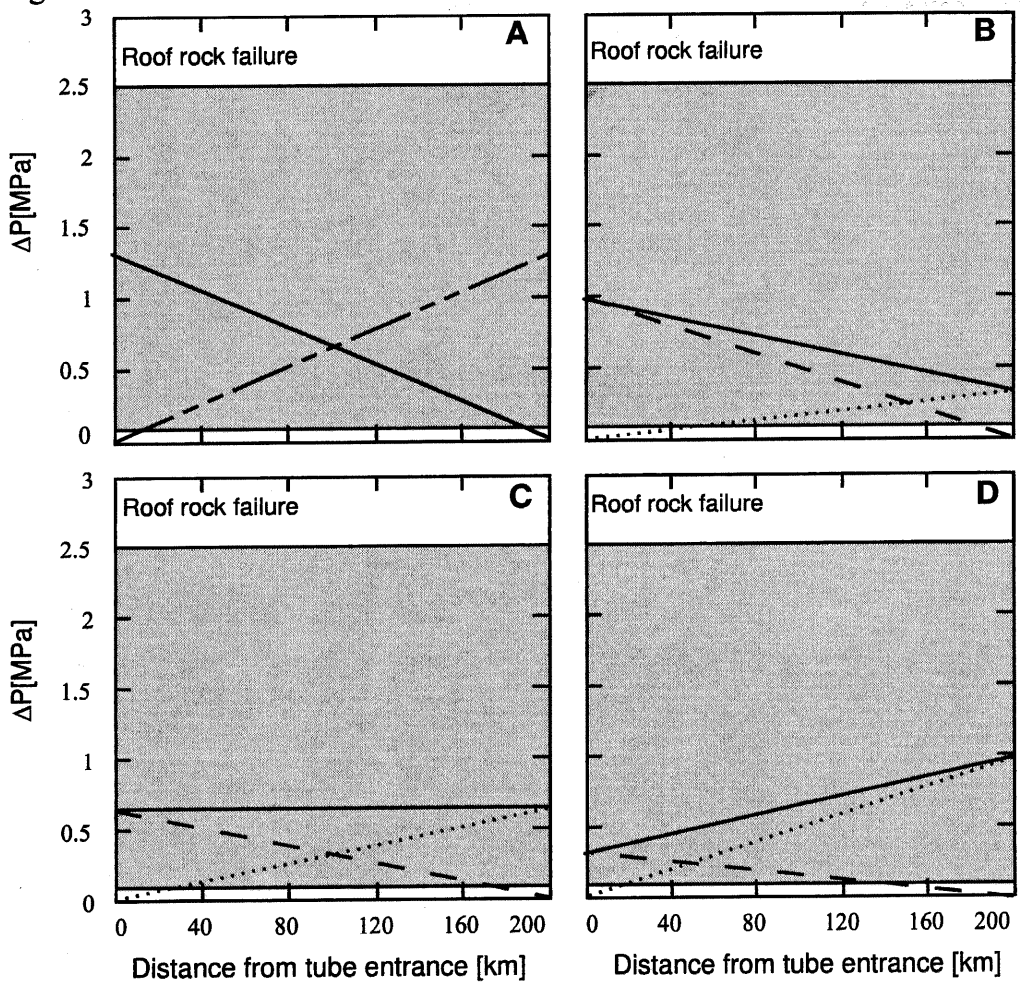
Roof rock failure
A
Roof rock failure
B
Roof rock failure
C
Roof rock failure
D
ΔP[MPa]
ΔP[MPa]
3
2.5
2
1.5
1
0.5
0
0
40
80
120
160
200
Distance from tube entrance [km]
Distance from tube entrance [km]

Figure 9.

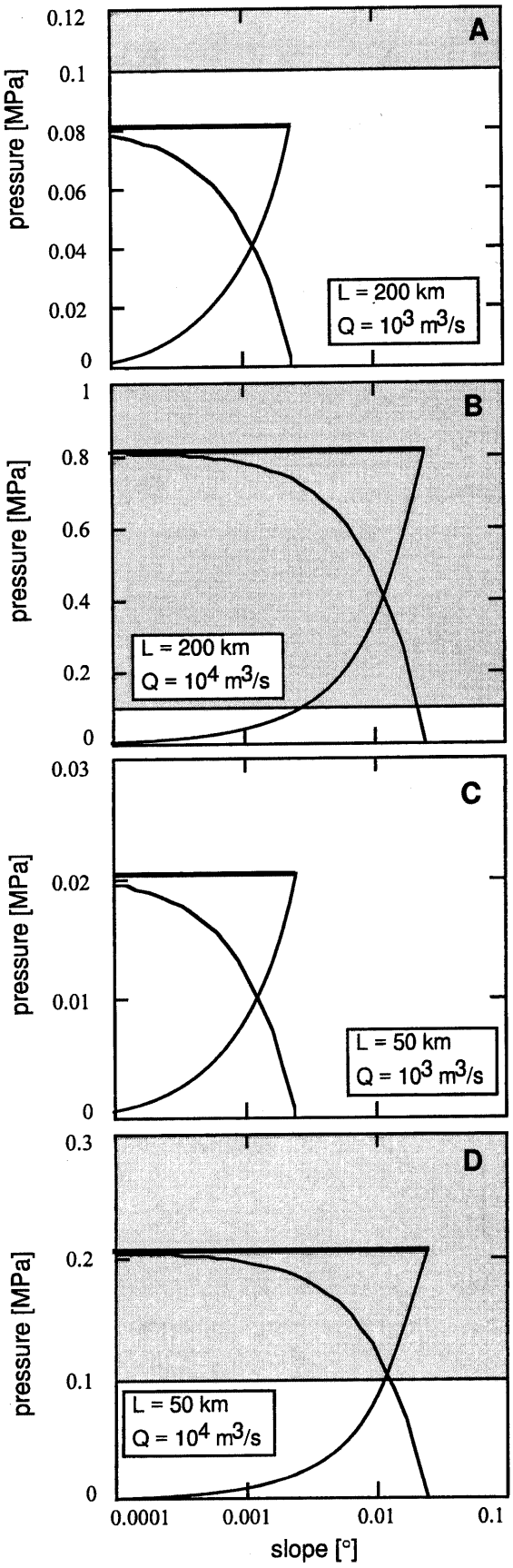
A
B
C
D
pressure [MPa]
0.12
0.1
0.08
0.06
0.04
0.02
0
L = 200 km
Q = 10^3 m^3/s
1
0.8
0.6
0.4
0.2
L = 200 km
Q = 10^4 m^3/s
0.03
0.02
0.01
L = 50 km
Q = 10^3 m^3/s
0.3
0.2
0.1
L = 50 km
Q = 10^4 m^3/s
0.0001
0.001
0.01
0.1
slope [°]

Figure 12a

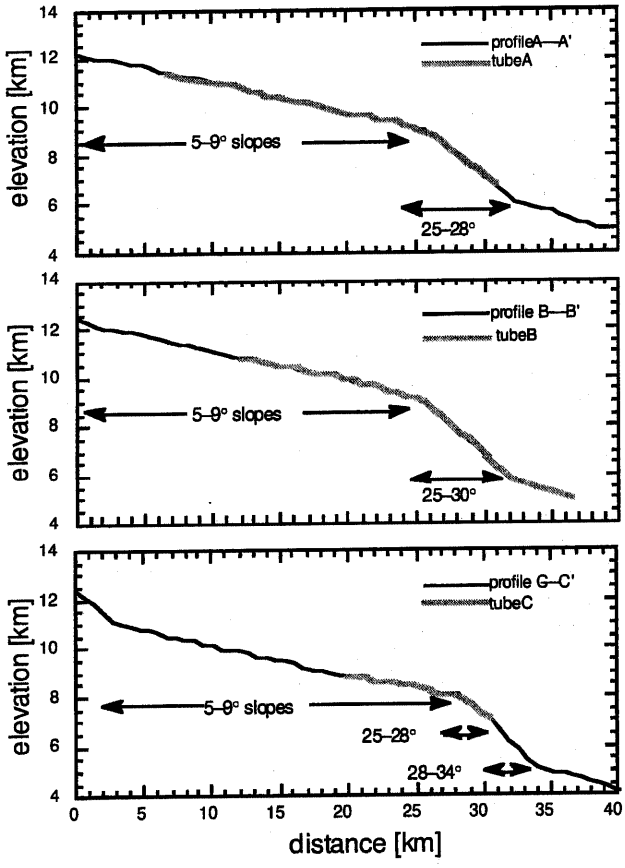

Figure 12b.

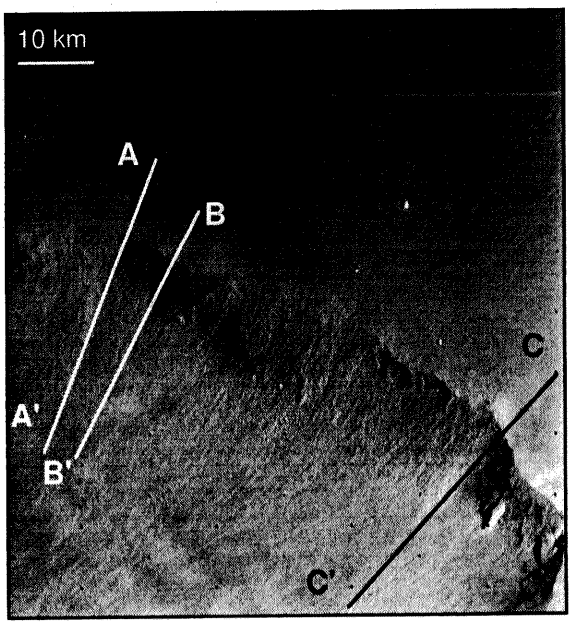

Figure 13.

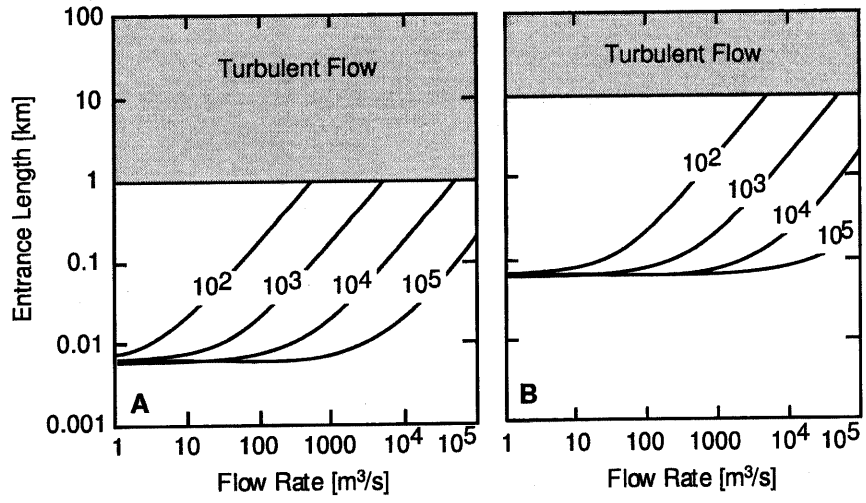

Figure 11.

Figure 14.

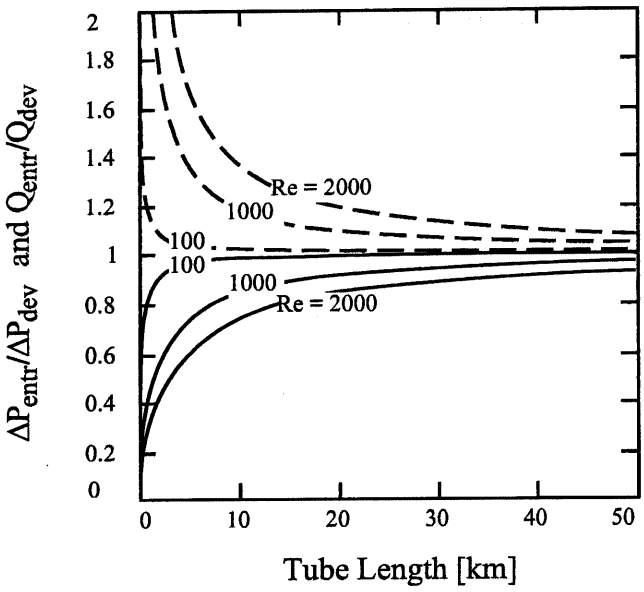
2
1.8
1.6
1.4
1.2
1
0.8
0.6
0.4
0.2
0
0
10
20
30
40
50
Re = 2000
1000
100
100
1000
Re = 2000
ΔP_entr/ΔP_dev and Q_entr/Q_dev
Tube Length [km]